Partial slip effect on non-aligned stagnation point nanofluid over a stretching convective surface

S. Nadeem[a)], Rashid Mehmood[a)†], and Noreen Sher Akbar[b)]

[a)] *Department of Mathematics, Quaid-i-Azam University* 45320, *Islamabad* 44000, *Pakistan*
[b)] *DBS&H, CEME, National University of Sciences and Technology, Islamabad, Pakistan*

(Received 6 April 2014; revised manuscript received 10 July 2014; published online 25 November 2014)

The present study inspects the non-aligned stagnation point nano fluid over a convective surface in the presence of partial slip. Two types of base fluids namely water and kerosene are selected with Cu nanoparticles. The governing physical problem is presented and transformed into a system of coupled nonlinear differential equations using suitable similarity transformations. These equations are then solved numerically using midpoint integration scheme along with Richardson extrapolation via Maple. Impact of relevant physical parameters on the dimensionless velocity and temperature profiles are portrayed through graphs. Physical quantities such as local skin frictions co-efficient and Nusselt numbers are tabularized. It is detected from numerical computations that kerosene-based nano fluids have better heat transfer capability compared with water-based nanofluids. Moreover it is found that water-based nanofluids offer less resistance in terms of skin friction than kerosene-based fluid. In order to authenticate our present study, the calculated results are compared with the prevailing literature and a considerable agreement is perceived for the limiting case.

Keywords: partial slip, non-aligned stagnation point, nanofluid, stretching convective surface

PACS: 47.50.–d, 47.50.Cd, 47.15.–x **DOI:** 10.1088/1674-1056/24/1/014702

1. Introduction

The notion of nanofluids has become a topic of global interest in the last few decades as they provide an effective way of improving heat transfer characteristics of fluids. It is expected that thermal conductivity of nanofluids is higher than that of common fluids.[1] Heat transfer fluids like water, oil, and glycols are extensively used in industrial and civil applications such as hot metal shears,[2] fire-resistance, air conditioning, electric cooling, etc. but they possess low thermal conductivity. In certain engineering processes like paper production, glass blowing, crystal growing, extrusion of plastic[3] and metal spinning, heat transfer rate at the stretching surface is dynamic since it is closely related to the quality of the final product. In order to overcome this deficiency, thermally conductive nano-meter sized particles (1–100 nm) are suspended in the base fluid to accelerate the heat transfer rate. Choi[4] devised the notable concept of nanofluids. Wongwises *et al.*[5] presented a critical analysis of convective heat transfer nanofluids. Leon *et al.*[6] broadly decorated the applications of nanofluids. Some useful studies emphasizing the utility of nanofluids can be found in Refs. [7]–[10]. Nanofluid flows over stretching surface are a topic of intense study these days. A great number of researchers have conducted independent studies to discuss the flow behavior of nanofluids under certain physical situations, e.g., Bachok *et al.*[11] monitored the stagnation-point flow over a stretching/shrinking sheet in a nanofluid. Anderson[12] presented a novel study on slip flow past a stretching surface. In another article, Hill *et al.*[13] focused on the nano boundary layer equation with nonlinear Navier boundary condition. Zhang *et al.*[14] deliberated a useful analysis to study the effect of slip condition on the MHD stagnation-point over a power-law stretching sheet. Viscous flow over a shrinking sheet with a second-order slip flow model is presented by Aziz *et al.*[15] Wang[16] examined the viscous flow due to a stretching sheet with surface slip and suction. Mukhopadhyay *et al.*[17] estimated the effects of partial slip on boundary layer flow past a permeable exponential stretching taking into account the thermal radiation. Recently, Das[18] inspected the slip flow and convective heat transfer of nanofluids over a permeable stretching surface and concluded that the increase in the slip velocity and nanoparticle volume fraction consequently increases the thermal boundary layer thickness. Yazdi *et al.*[19] conferred the slip MHD liquid flow over nonlinear permeable stretching surface with chemical reaction. Pop *et al.*[20] piloted a valuable study to discuss the convective heat transfer in the flow of a water-based nanofluid over a stretching surface. Some noteworthy studies related to the present topic can be found in Refs. [21]–[35]. To the best of our knowledge, no one so far has discussed the non-aligned stagnation point nanofluid flow with partial slip and convective heat transfer over a stretching surface. Hence, our motivation is to discuss the partial slip effect on a nanofluid over a stretching convective surface when the fluid strikes the wall in an oblique manner.

†Corresponding author. E-mail: rmqau@hotmail.com

© 2015 Chinese Physical Society and IOP Publishing Ltd

2. Mathematical formulation

Consider the steady oblique stagnation point flow of a nano fluid over a stretching surface which strikes the surface at $y = 0$. Two types of base fluids namely water and kerosene are selected with Cu nanoparticles. The base fluid and the nanoparticles are in thermal equilibrium. Two forces of equal magnitude are applied in opposite directions to keep the surface stretched. The fluid lodges the entire half plane $y > 0$. It is presumed that the surface has temperature T_f, and free stream temperature T_∞.

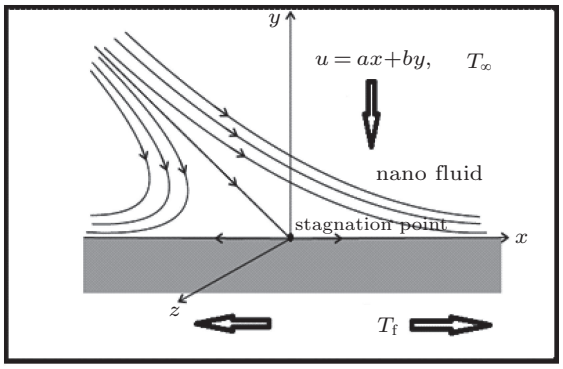


Fig. 1. Physical description of the problem.

Under these assumptions, the equations governing the flow and heat phenomenon are[9–11,20,21]

$$\frac{\partial u^*}{\partial x^*} + \frac{\partial v^*}{\partial y^*} = 0, \tag{1}$$

$$u^*\frac{\partial u^*}{\partial x^*} + v^*\frac{\partial u^*}{\partial y^*} + \frac{1}{\rho_{nf}}\frac{\partial p^*}{\partial x^*} = \upsilon_{nf}\nabla^{*2}u^*, \tag{2}$$

$$u^*\frac{\partial v^*}{\partial x^*} + v^*\frac{\partial v^*}{\partial y^*} + \frac{1}{\rho_{nf}}\frac{\partial p^*}{\partial y^*} = \upsilon_{nf}\nabla^{*2}v^*, \tag{3}$$

$$u^*\frac{\partial T^*}{\partial x^*} + v^*\frac{\partial T^*}{\partial y^*} = \alpha^*_{nf}\frac{\partial^2 T^*}{\partial y^{*2}}, \tag{4}$$

where u^* and v^* are the velocity components along the coordinate axis respectively. T^* is the temperature, υ_{nf} is the effective kinematic viscosity, and α_{nf} is the effective thermal diffusivity of nanofluid. The physical properties of nanofluids restricted to spherical nanoparticles can be stated as the cartel features of based fluids and nanoparticles in terms of particle volume fraction as follows:[20,21]

$$\begin{cases} \rho_{nf} = (1-\phi)\rho_f + \phi\rho_s, \quad \mu_{nf} = \dfrac{\mu_f}{(1-\phi)^{2.5}}, \\ (\rho C_p)_{nf} = (1-\phi)(\rho C_p)_f + \phi(\rho C_p), \quad \upsilon_{nf} = \dfrac{\mu_{nf}}{\rho_{nf}}, \\ k_{nf} = k_f\left\{\dfrac{k_s + 2k_f - 2\phi(k_f - k_s)}{k_s + 2k_f + \phi(k_f - k_s)}\right\}, \quad \alpha_{nf} = \dfrac{k_{nf}}{(\rho C_p)_{nf}}, \end{cases} \tag{5}$$

where k_{nf} is the thermal conductivity, $(\rho C_p)_{nf}$ is the heat capacity, and Φ is the solid volume fraction of nanofluid.

The appropriate boundary conditions are[18,22]

$$\begin{cases} u^* = cx^* + N\mu\dfrac{\partial u^*}{\partial y^*}, \\ -k\dfrac{\partial T^*}{\partial y^*} = h_f(T_f - T^*), \quad \text{at} \quad y^* = 0, \\ u^* = ax^* + by^*, \quad T \to T_\infty, \ \text{as} \ \ y^* \to \infty, \end{cases} \tag{6}$$

where a, b, and c are positive constants with dimensions of inverse time, N is a slip constant, h_f is the convective heat transfer coefficient, and $c > 0$ is the stretching rate. By using

$$\begin{cases} x = x^*\sqrt{\dfrac{c}{\upsilon_f}}, \quad y = y^*\sqrt{\dfrac{c}{\upsilon_f}}, \quad u = \dfrac{1}{\sqrt{\upsilon_f c}}u^*, \\ u = \dfrac{1}{\sqrt{\upsilon_f c}}u^*, \quad p = \dfrac{1}{(\rho\upsilon)_f c}p^*, \quad T = \dfrac{T^* - T_\infty}{T_f - T_\infty}, \end{cases} \tag{7}$$

Equations (1)–(4) yield

$$\frac{\partial u}{\partial x} + \frac{\partial v}{\partial y} = 0, \tag{8}$$

$$u\frac{\partial u}{\partial x} + v\frac{\partial u}{\partial y} + \frac{\rho_f}{\rho_{nf}}\frac{\partial p}{\partial x} = \frac{\upsilon_{nf}}{\upsilon_f}\nabla^2 u, \tag{9}$$

$$u\frac{\partial v}{\partial x} + v\frac{\partial v}{\partial y} + \frac{\rho_f}{\rho_{nf}}\frac{\partial p}{\partial y} = \frac{\upsilon_{nf}}{\upsilon_f}\nabla^2 v, \tag{10}$$

$$u\frac{\partial T}{\partial x} + v\frac{\partial T}{\partial y} = \frac{\alpha_{nf}}{\upsilon_f}\frac{\partial^2 T}{\partial y^2}. \tag{11}$$

Introducing the stream function relations

$$u = \frac{\partial\psi}{\partial y}, \quad v = \frac{-\partial\psi}{\partial x}, \tag{12}$$

and making use of Eq. (12) in Eqs. (8)–(11), and eliminating the pressure by using the fact $p_{xy} = p_{yx}$ yield

$$\frac{1}{(1-\phi)^{2.5}}\nabla^4\psi + \left[(1-\phi) + \phi\frac{\rho_s}{\rho_f}\right]\frac{\partial(\psi, \nabla^2\psi)}{\partial(x,y)} = 0, \tag{13}$$

$$\frac{\partial\psi}{\partial y}\frac{\partial T}{\partial x} - \frac{\partial\psi}{\partial x}\frac{\partial T}{\partial y} = \frac{\alpha_{nf}}{\upsilon_f}\frac{\partial^2 T}{\partial y^2}. \tag{14}$$

Finally, we search for solution of Eqs. (13) and (14) of the form[22]

$$\psi = xf(y) + g(y), \quad T = \theta(y), \tag{15}$$

where $f(y)$ and $g(y)$ represent the normal and tangential components of flow respectively. Substituting Eq. (15) into Eqs. (13) and (14), we obtain

$$\frac{1}{(1-\phi)^{2.5}}f''' + \left[(1-\phi) + \phi\frac{\rho_s}{\rho_f}\right](ff'' - f'^2) + C_1 = 0, \tag{16}$$

$$\frac{1}{(1-\phi)^{2.5}}g''' + \left[(1-\phi) + \phi\frac{\rho_s}{\rho_f}\right](fg'' - f'g') + C_2 = 0, \tag{17}$$

$$\frac{k_{nf}}{k_f}\theta'' + Pr\left[(1-\phi) + \phi\frac{(\rho C_p)_s}{(\rho C_p)_f}\right](f\theta') = 0, \tag{18}$$

and the boundary conditions

$$\begin{cases} f(0) = 0, \quad f'(0) = 1 + \lambda f''(0), \quad f'(\infty) = a/c, \\ g(0) = 0, \quad g'(0) = \lambda g''(0), \quad g''(\infty) = \gamma = b/c, \\ \theta'(0) = -Bi(1 - \theta(0), \quad \theta(\infty) = 0, \end{cases} \tag{19}$$

where $Pr = (\mu C_p)_f/k_f$ is the Prandtl number, $\lambda = N\rho\sqrt{cv}$ is the slip parameter and $Bi = (h/k)\sqrt{v/c}$ is the Biot number. Using the boundary condition (19), we obtain

$$C_1 = \left[(1-\phi) + \phi\frac{\rho_s}{\rho_f}\right](a/c)^2,$$
$$C_2 = -\delta\gamma\left[(1-\phi) + \phi\frac{\rho_s}{\rho_f}\right],$$

where we have used the datum that $f(y)$ behaves as $(a/c)y+\delta$ as y goes to infinity. Here δ represents the boundary layer displacements constant which needs to be computed.

Introducing

$$g'(y) = \gamma h(y), \tag{20}$$

equations (16)–(19) give

$$\begin{cases} \dfrac{1}{(1-\phi)^{2.5}}f''' + \left[(1-\phi) + \phi\dfrac{\rho_s}{\rho_f}\right] \\ (ff'' - f'^2 + (a/c)^2) = 0, \\ \dfrac{1}{(1-\phi)^{2.5}}h'' + \left[(1-\phi) + \phi\dfrac{\rho_s}{\rho_f}\right](fh' - f'h - \delta) = 0, \\ \dfrac{k_{nf}}{k_f}\theta'' + Pr\left[(1-\phi) + \phi\dfrac{(\rho C_p)_s}{(\rho C_p)_f}\right](f\theta') = 0, \\ f(0) = 0, \quad f'(0) = 1 + \lambda f''(0), \\ h(0) = \lambda h'(0), \quad \theta'(0) = -Bi(1-\theta(0), \\ f'(\infty) = a/c, \quad h'(\infty) = 1, \quad \theta(\infty) = 0. \end{cases} \tag{21}$$

Physical quantities of interest are the shear stress and local heat flux at the wall which are given by

$$\tau_w = \frac{1}{(1-\phi)^{2.5}}[xf''(0) + \gamma h'(0)],$$
$$q_w = -\frac{k_{nf}}{k_f}\theta'(0). \tag{22}$$

The position x_s of attachment of dividing streamline is determined by zero wall shear stress, i.e.,

$$x_s = \frac{-\gamma h'(0)}{f''(0)}. \tag{23}$$

One can observe that the point of stagnation is independent of particle volume fraction of nanoparticles.

3. Method of solution

The system of coupled non-linear ordinary differential equations along with the boundary conditions (21) is complicated in nature, so a numerical solution would be an obvious choice. Keeping this in mind, a very efficient computational software known as Maple 15 is used to obtain numerical results as well as graphical outputs. The governing system is solved numerically using the midpoint integration scheme along with Richardson's extrapolation.[27–29] This involves the transformation of the governing system of equations into a set of first-order non-linear differential equations which are then conveniently integrated to achieve the required solutions. The problem of semi-infinite domain [0, ∞) is generously transformed into such appropriate finite domain of y, i.e., [0, y_∞), where y_∞ should be large enough that the numerical solutions would approach the asymptotic behavior at the infinite boundaries. A mesh size of $\Delta h = 0.001$ was found enough for a convergence criterion of 10^{-6} in almost all cases. In order to confirm the accuracy of our numerical solutions, results are obtained in the absence of nanoparticles, i.e., for the case of pure fluid when ($\Phi_0 = 0$) and they are found to be in good agreement with those of Pop *et al.*[22] and Gupta *et al.*[25] (see Table 1).

Table 1. Comparison with the previous existing literature when $\lambda = 0 = \Phi$.

	$f''(0)$			$h'(0)$	
a/c	Present	Gupta *et al.*[25]	Pop *et al.*[22]	Present	Pop *et al.*[22]
0.1	−0.96938	−0.9694	−0.96938	0.26332	0.26278
0.3	−0.84942		−0.84942	0.60631	0.60573
0.8	−0.29938		−0.29938	0.93472	0.93430
1.0			0.0	1.0	1.0
2.0	2.01750	2.01750	2.01750	1.16521	1.16489
3.0	4.72928	4.72930	4.72928	1.23465	1.23438

4. Results and discussion

For the sake of analysis, we have conducted numerical computations against various values of stretching ratio a/c, slip parameter λ, and nanoparticle volumetric concentration on velocity and temperature profiles. Figures 2–7 are plotted to highlight these effects. Figures 2 and 3 show the impact of stretching parameter a/c and slip parameter λ on normal flow $f(y)$ and velocity profile $f'(y)$ for the case of pure fluid ($\Phi = 0$) and nanofluid ($\Phi = 0$). From Figs. 2(a) and 2(b), it is observed that the normal component of the flow $f(y)$ increases with the increase in stretching ratio a/c, whereas it tends to decrease with increasing slip factor λ. Moreover, it is apparent that the normal component of the flow $f(y)$ is higher in magnitude for the case of pure fluid when compared with the nanofluid. Figure 3(a) displays that the normal component of the velocity $f'(y)$ increases as we increase stretching ratio a/c and it is apparent in the boundary layer region. This is due to the fact that when stretching ratio a/c increases, it causes the free stream velocity ax of the external fluid to exceed the stretching velocity cx of the stretching surface. Figure 3(b) depicts that with the increase in slip parameter λ, the normal component of the velocity $f'(y)$ decreases. The physical reasoning behind it could be that when the slip factor is increased, it leads the fluid particles near the stretching surface to move swiftly which consequently decreases the normal fluid velocity. Figures 4(a) and 4(b) study the influence of stretching parameter a/c and slip parameter λ on tangential flow component $h(y)$. It is easily noticeable from these figures that both these parameters have a positive influence on

tangential flow component $h(y)$. This is in good agreement with the physical situation because an increase in the stretching rate or increase in the slip factor ultimately favours the tangential flow due to its direction. Behavior of the tangential velocity component $h'(y)$ against stretching parameter a/c and slip factor λ is expressed through Figs. 5(a) and 5(b). It is found that tangential velocity $h'(y)$ rises with stretching parameter a/c. Further, nanoparticle volumetric concentration Φ causes an initial increase in the tangential velocity $h'(y)$ (see Fig. 5(a)). From Fig. 5(b), it is evident that an increase in the slip factor, leads to a reduction in tangential velocity $h'(y)$. In addition, it is also found that the magnitude of the tangential velocity $h'(y)$ is higher for the case of nanofluid within the boundary layer region when compared with the pure fluid. Figures 6 and 7 give us an idea about how the temperature profile $\theta(y)$ reacts against various values of stretching parameter a/c, slip parameter λ, and nanoparticle volumetric concentration Φ. Figure 6(a) indicates that when we increase the stretching parameter a/c, temperature profile $\theta(y)$ drops. Furthermore, it also appears that with insertion

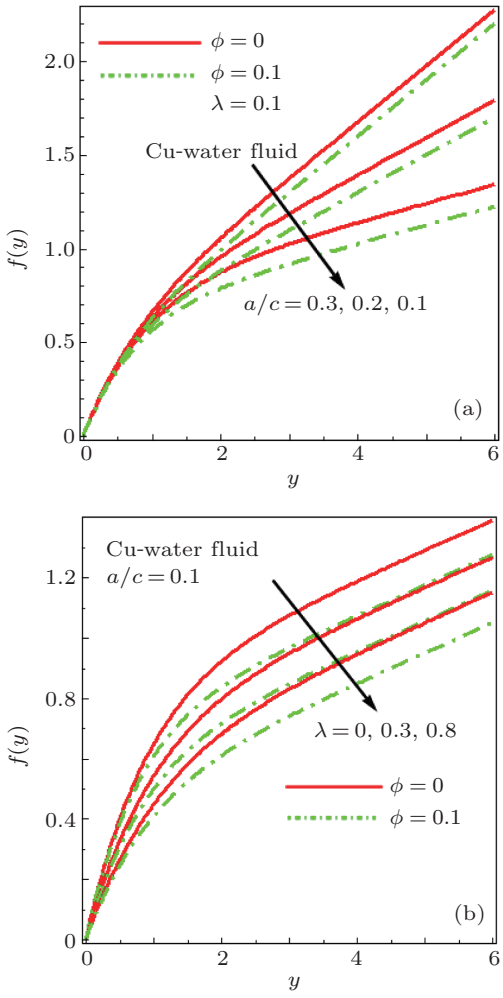


Fig. 2. (color online) Velocity profile $f(y)$ against a/c (a) and λ (b).

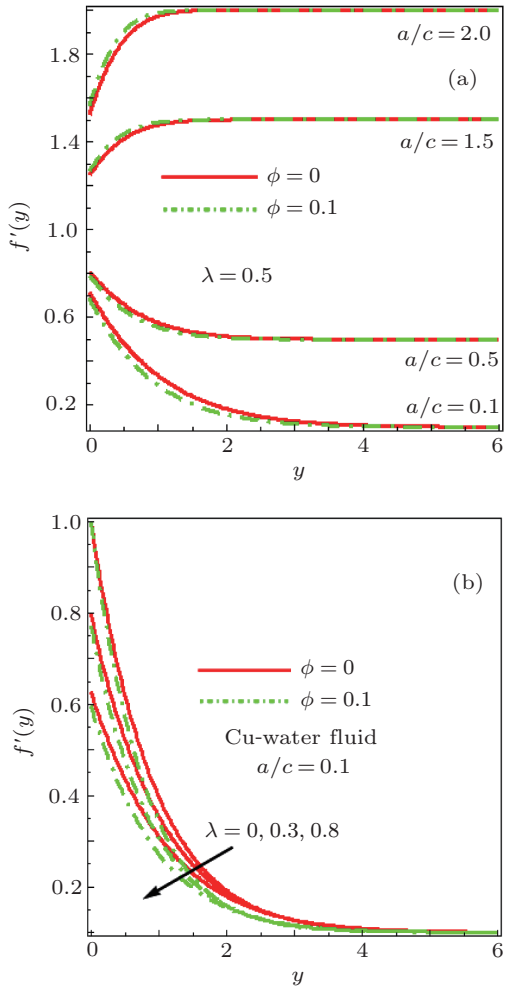


Fig. 3. (color online) Velocity profile $f'(y)$ against a/c (a) and λ (b).

of nanoparticles, magnitude of temperature profile $\theta(y)$ rises in comparison to the pure fluid. This is due to the inclusion of Cu nanoparticles; these tiny nano particles have a lot higher thermal conductivity and comparatively low specific heat in comparison to the base fluid which consequently gives higher temperature at the surface. Figure 6(b) describes that slip parameter λ causes an increase in the temperature profile $\theta(y)$. Figures 6(a) and 6(b) specify that with the increase in Biot number Bi and nanoparticle volumetric concentration Φ, temperature profile $\theta(y)$ rises substantially. Since Biot number Bi involves the heat transfer coefficient so an increase in Biot number results in an increase in heat transfer coefficient which consequently enhances the fluid temperature $\theta(y)$. It can also be perceived that $\theta(y)$ is higher for nanofluid than pure fluid, close to the stretching convective surface. Finally the streamline pattern of the present problem for several shears in the flow is traced through Figs. 8(a)–8(c). It is found that streamlines are tilted towards the left side of the origin for positive shear rate and it falls on the right side when the value of shear rate is taken to be negative. Moreover the streamline $\psi = 0.0$ meets the wall at $x = x_s$, the point of stagnation.

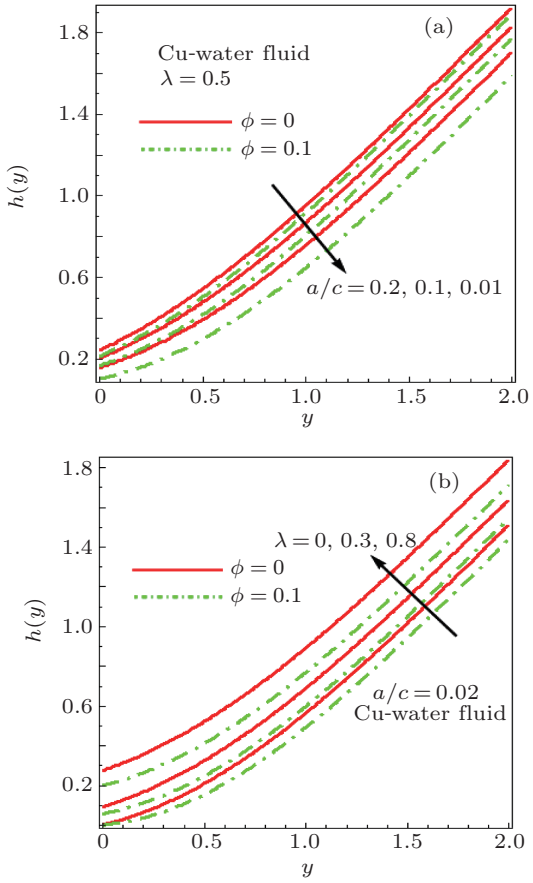


Fig. 4. (color online) Velocity profile $h(y)$ against a/c (a) and λ (b).

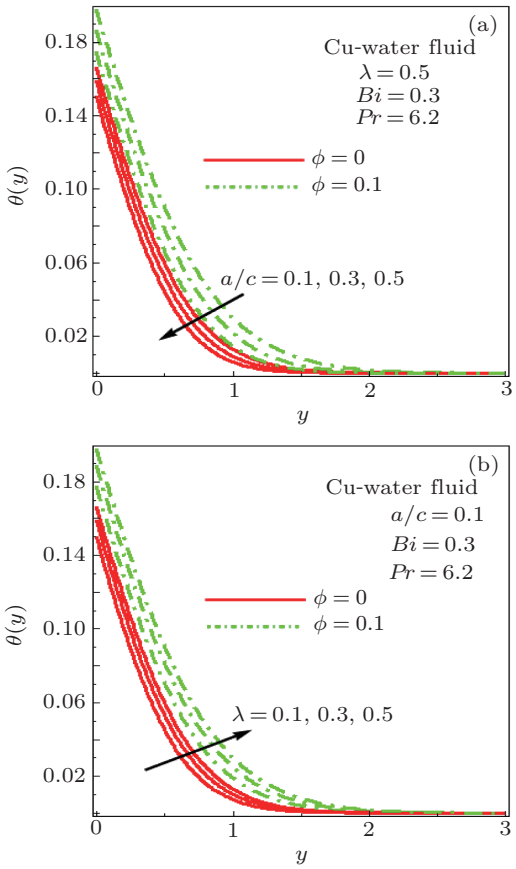


Fig. 6. (color online) Temperature profile $\theta(y)$ against a/c (a) and λ (b).

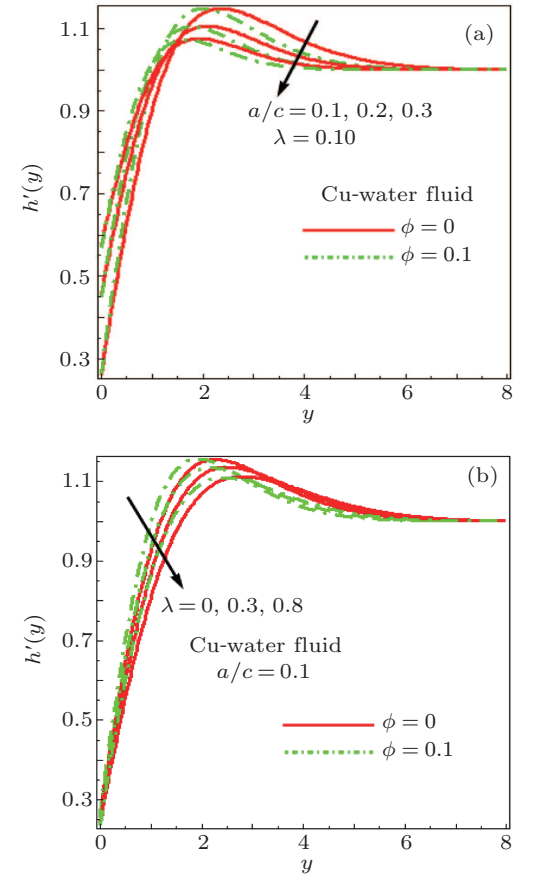


Fig. 5. (color online) Velocity profile $h'(y)$ against a/c (a) and λ (b).

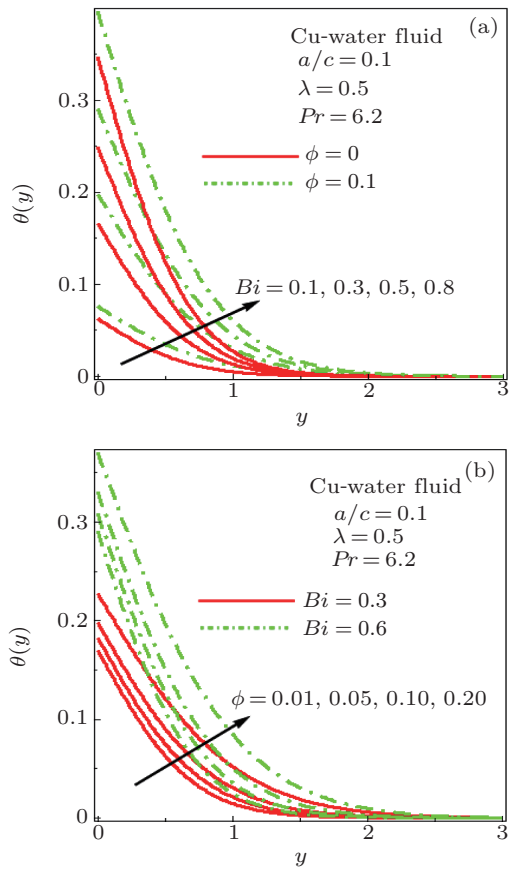


Fig. 7. (color online) Temperature profile $\theta(y)$ against Bi (a) and ϕ (b).

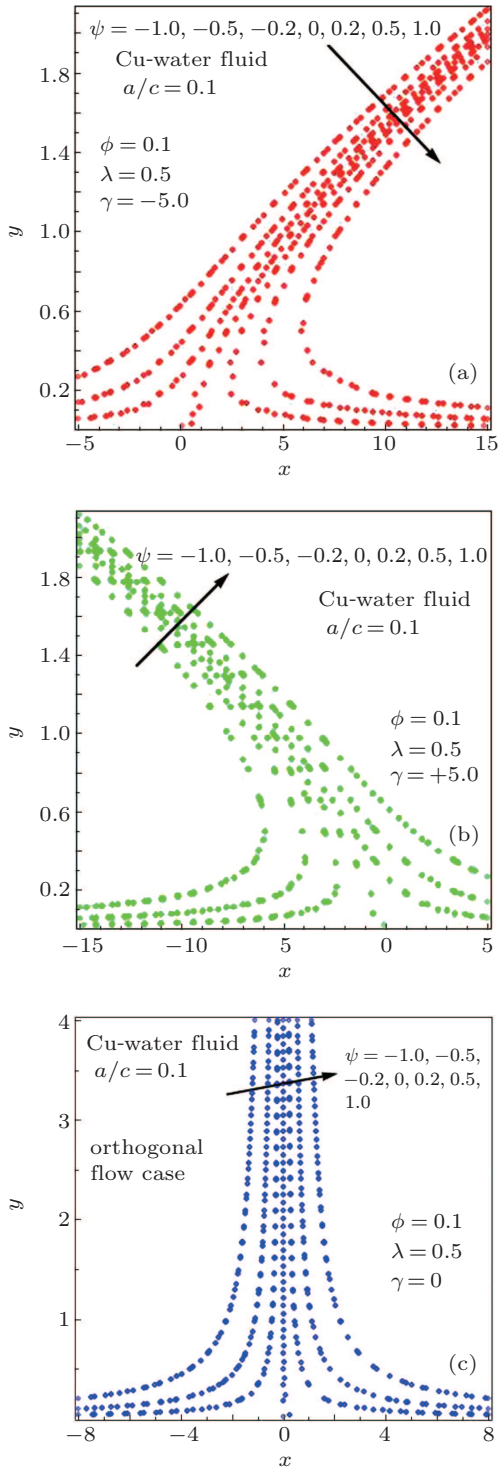


Fig. 8. (color online) Streamline patterns for $\gamma = -5.0$ (a), $\gamma = +5.0$ (b), and $\gamma = 0.0$ (c).

Table 2 gives the thermo physical properties of water- and kerosene-based fluids with selected Cu nanoparticles.[9–11] Tables 1, 3, 4 are set to classify the influence of stretching ratio a/c, slip parameter λ, Biot number Bi and nanoparticles volumetric concentration Φ on local skin friction and heat flux. Table 1 confirms that our present results are in good agreement with those of Pop *et al.*[22] and Gupta *et al.*[25] for the case of pure fluid i.e., when $\Phi = 0$. Tables 3 and 4 are developed to compute the local skin frictions and heat flux at the stretching convective surface for water- and kerosene-based fluids respectively. These are some of the key findings. First of all, it is noticeable from both these tables that boundary layer displacement constant δ continuously decreases with the increase in stretching parameter a/c, slip parameter λ, and nanoparticle volumetric concentration. Besides, a slightly greater value of boundary layer displacement constant δ is recorded for water-based fluid than kerosene-based fluid. This is perhaps due to the fact that kerosene-based fluids are more viscous in nature than water-based fluids and offer more resistance to the flow. It is also obvious from these tables that increasing nanoparticle volumetric concentration results in an increase in both normal and tangential components of the local skin friction for water as well as kerosene-based fluid. Increasing stretching parameter a/c descents the normal skin friction component while it raises the tangential component of the local skin friction for both types of base fluids. The tabulated results also revealed that when we increase the slip parameter λ local skin friction components gradually declines. This has clear physical justification as increased slip causes the stretched surface to offer less resistance which consequently decays local skin friction and heat transfer rate. Heat transfer rate at the stretching convective surface increases when stretching ratio a/c, Biot number Bi, and nanoparticles volumetric concentration increases for water- and kerosene-based fluids while it portrays a decreasing behavior for the slip parameter λ. From these results it can be perceived that nanoparticles can certainly improve the heat transfer rate at the surface. Moreover, it is also observed that for large values of Biot number Bi, local heat flux at the wall also increases which is clearly because larger Biot numbers mean higher heat transfer co-efficients which helps in better heat transfer rate at the stretching convective surface. Further it is worth mentioning here that kerosene-based fluid has shown better heat transfer ability compared to the water-based fluid. These results are well justified with the fact that kerosene-based fluid has less thermal conductivity and higher Prandtl number Pr compared with traditional water-based fluid.

Table 2. Thermal characteristics of water and kerosene with Cu nanoparticles.[9,11,20]

Physical properties	Kerosene	Water	Cu
ρ/(kg/m^3)	783	997.1	8933
C_p/(J/kg)	2090	4179	385
k/(W/m)	0.15	0.613	400
Pr	15.6	6.2	–

Table 3. Numerical values of local skin friction co-efficient and local heat flux for Cu–water-based fluid.

Φ	a/c	λ	Bi	δ	$\frac{-1}{(1-\phi)^{2.5}}f''(0)$	$\frac{1}{(1-\phi)^{2.5}}h'(0)$	$-\frac{k_{\rm nf}}{k_{\rm f}}\theta'(0)$
0.01	0.1	0.2	0.3	0.682579	0.787713	0.265072	0.260436
0.10				0.587198	1.109253	0.335254	0.326348
0.20				0.563879	1.530281	0.449593	0.413112
0.10	0.1	0.2	0.3	0.587198	1.109253	0.335254	0.326348
	0.3			0.364328	0.968819	0.697707	0.329180
	0.5			0.220759	0.756543	0.856601	0.332380
0.1	0.1	0.1	0.3	0.625587	1.265146	0.339529	0.328772
		0.3		0.555491	0.990752	0.330553	0.324231
		0.5		0.505266	0.820951	0.320837	0.320645
0.1	0.1	0.5	0.1				0.123075
			0.2				0.228817
			0.3				0.320645

Table 4. Numerical values of local skin friction co-efficient and local heat flux for Cu-kerosene-based fluid.

Φ	a/c	λ	Bi	δ	$\frac{-1}{(1-\phi)^{2.5}}f''(0)$	$\frac{1}{(1-\phi)^{2.5}}h'(0)$	$-\frac{k_{\rm nf}}{k_{\rm f}}\theta'(0)$
0.01	0.1	0.2	0.3	0.674154	0.794626	0.265003	0.282084
0.10				0.546591	1.163893	0.334650	0.361085
0.20				0.511546	1.632064	0.448432	0.468682
0.10	0.1	0.2	0.3	0.546591	1.163893	0.334650	0.361085
	0.3			0.338032	1.016275	0.692649	0.362108
	0.5			0.204327	0.793264	0.847970	0.363424
0.1	0.1	0.1	0.3	0.584221	1.336072	0.339269	0.362595
		0.3		0.515771	1.034593	0.329598	0.359763
		0.5		0.467362	0.851543	0.319243	0.357508
0.1	0.1	0.5	0.1				0.128226
			0.2				0.247064
			0.3				0.357508

5. Conclusions

The present study provides the influence of partial slip on non-aligned stagnation point flow of a nanofluid over a stretching convective surface. The main findings of the study can be summarized as follows.

Within the boundary layer region, normal flow and velocity decreases with the increase in the slip parameter while it increases with the increase in stretching ratio.

Effect of stretching ratio and slip parameter on tangential flow is positive, whereas tangential velocity responded in an opposite manner for both these parameters.

Boundary layer displacement constant δ tends to decrease with an increase in stretching ratio, slip parameter and nanoparticle volume fraction.

Insertion of nanoparticles drops both normal and tangential velocity components and increases the temperature profile.

With an increase in nanoparticle volume fraction, local skin friction and heat flux at the wall increases. Moreover, kerosene-based fluids have shown higher heat transfer rates compared with the water-based fluids.

References

[1] Wang X, Xu X and Choi U S 1999 *J. Therm. Phys. Heat. Trans.* **13** 474

[2] Altan T, Oh S and Gegel H 1983 *Metal Forming Fundamentals and Applications* (New York: Asm Intl)

[3] Tadmor Z and Klein I 1970 *Engineering Principles of Plasticating Extrusion* (New York: van Nostrand Reinhold)

[4] Choi U S 1995 *ASME FED* **231** 99

[5] Daungthongsuk W and Wongwises S 2007 *Renew Sustain Energy Rev.* **11** 797

[6] Wong K F V and Leon O D 2010 *Adv. Mech. Eng.* **2010** 519659

[7] Eastman J A, Choi S U S, Li S, Yu W and Thompson L J 2007 *Appl. Phys. Lett.* **78** 718

[8] Xuan Y M and Li Q 2003 *ASME J. Heat. Transfer* **125** 151

[9] Wen D and Ding Y 2004 *Int. J. Heat Mass Transfer* **47** 5181

[10] Hwang K S, Jang S P and Choi S U 2009 *Int. J. Heat Mass Transfer* **52** 193

[11] Bachok N, Ishak A and Pop I 2011 *Nanoscale Res. Lett.* **6** 623

[12] Andersson H I 2002 *Acta Mech.* **158** 121

[13] Matthews M T and Hill J M 2007 *J. Math Anal. Appl.* **333** 381

[14] Zhu J, Zheng L and Zhang X 2010 *Appl. Math. Mech.* **31** 439

[15] Fang T, Yao S, Zhang J and Aziz A 2010 *Commun. Nonlinear Sci. Numer. Simul.* **15** 1831

[16] Wang C Y 2009 *Nonlinear Anal. Real World Appl.* **10** 375

[17] Mukhopadhyay S and Gorla R S R 2012 *Heat Mass Transfer* **48** 1773

[18] Das K 2012 *Computers & Fluids* **64** 34

[19] Yazdi M H, Abdullah S, Hashim I and Sopian K 2011 *Int. J. Heat Mass Transfer* **54** 3214

[20] Vajravelu K, Prasad K V, Lee J, Lee C and Pop I 2011 *Int. J Therm. Sci.* **50** 843

[21] Maxwell-Garnett J C 1904 *Philosophical Transactions of the Royal Society A* **203** 385
[22] Labropuolu F, Li D and Pop I 2010 *Int. J. Therm. Sci.* **49** 1042
[23] Das K 2012 *Heat Mass Transfer* **48** 767
[24] Nadeem S, Mehmood R and Akbar N S 2013 *J. Taiwan Inst. Chem. Engnrs.* **44** 586
[25] Mahapatra and Gupta 2002 *Heat Mass Transfer* **38** 517
[26] Hamad M A A, Uddin M J and Ismail A I M 2012 *Int. J. Heat Mass Transer* **55** 1355
[27] Ascher U, Mattheij R and Russell R 1995 *SIAM Classics in Appl. Math.* **13** 327
[28] Ascher U and Petzold L 1998 *SIAM* (Philadelphia)
[29] Noghrehabadi A, Ghalambaz M and Samimi A 2013 *J. Comput. Appl. Research Mech. Eng.* **2** 45
[30] Fang T G, Tao H and Zhong Y F 2012 *Chin. Phys. Lett.* **29** 114703
[31] Nadeem S and Abdul R 2012 *Chin. Phys. Lett.* **29** 124701
[32] Swati M 2013 *Chin. Phys. B* **22** 074701
[33] Swati M 2013 *Chin. Phys. B* **22** 114702
[34] Ebaid A, El-arabawy A H and Nader Y 2013 *Int. J. Diff. Eqs.* **2013** 865464
[35] Ebaid A and Wazwaz A M 2014 *J. Comput. Theor. Nanosci.* **11** 178
[36] Ellahi R, Rahman S U, Nadeem S and Akbar N S 2014 *J. Comput. Theor. Nanosci.* **11** 1156